This article has been accepted for publication in a future issue of this journal, but has not been fully edited. Content may change prior to final publication. Citation information: DOI 10.1109/TMAG.2014.2358199, IEEE Transactions on Magnetics

Novel Electrical Machines Having Separate PM Excitation Stator

Z. Q. Zhu, *Fellow, IEEE*, Z. Z. Wu, D. J. Evans, and W. Q. Chu
Department of Electronic and Electrical Engineering, University of Sheffield, Sheffield S1 3JD, U.K.

***Abstract*— In this paper, novel electrical machines having a separate permanent magnet (PM) excitation stator are proposed based on a partitioned stator (PS) flux reversal (FR) PM (FRPM) machine. Different from the conventional FRPM machines with single stator, the PS-FRPM machines have two stators with PMs surface-mounted in one stator and the armature windings located in another stator. This paper investigates the electromagnetic performance of PS-FRPM machines with 12/10, 12/11, 12/13 and 12/14 stator/rotor-pole, together with the influence of leading design parameters. The torque characteristics of PS-FRPM machines are quantitatively compared with the conventional FRPM machines based on their globally optimized designs. It shows that the PS-FRPM machines can generally produce higher torque when the PMs are thicker and exhibit > 56% higher torque density than that of the conventional FRPM machines. Even compared under the same PM volume, the proposed PS-FRPM machines can have larger torque due to better utilization of the inner space. The investigation is validated by both finite element and experimental results.**

***Index Terms*— Flux reversal, partitioned stator, permanent magnet, surface-mounted, torque density.**

I. Introduction

Thanks to developments of permanent magnet (PM) materials, electrical machines equipped with PM excitation exhibit high efficiency due to elimination of excitation copper loss and high torque density especially when high energy product PMs, *e.g*. NdFeB, is employed [1]. Compared with rotor-PM brushless machines in which the PMs are located in the rotor, stator-PM brushless machines having PMs placed in the stator offer advantages such as easier management of PM temperature as well as simple and robust rotor [2][3]. However, stator-PM machines also have drawbacks. One of the drawbacks is manufacturing challenge. For doubly-salient [4], biased flux [5] and switched flux [6] PM machines with PMs placed in the stator yoke or between stator teeth, their stator core is not one piece but consisted of several pieces. Hence, it is more difficult to make and assemble [7]. The large repulsive force between adjacent PMs makes the assembly even more challenging. For flux reversal (FR) PM (FRPM) machines [8], although it is easier to make the stator core, it is hard to mount PMs on the tooth surfaces due to repulsive force between the adjacent PMs having same polarities, as shown in Fig. 1(a). More importantly, in all the stator-PM machines, both PMs and armature windings are located in the stator. The introduction of PMs on the stator causes consequent reduction of the slot area for armature windings when the air-gap diameter is fixed. Hence, the torque density may be compromised.

One of the methods to increase the torque density is to employ a double-stator configuration [9]-[12], which utilizes the inner space to accommodate an inner stator. The outer and inner stators are similar in [12]. Thus, the manufacturing challenges and the geometric confliction between the PMs and armature windings remain the same in stator-PM machines having double stators.

In this paper, a novel electrical machine having a separate PM excitation stator is proposed based on the concept of a partitioned stator (PS) FRPM (PS-FRPM) machine, as shown in Fig. 1(b). The proposed PS-FRPM machine has two stators, *i.e*. one stator having the armature windings and another stator having the PMs. In Fig. 1(b), the armature windings are on the outer stator, while the PMs are on the inner stator. Compared with the conventional double-stator configuration, the PMs and the armature windings in PS-FRPM machines are geometrically separated. The inner stator of PS-FRPM machine become a typical surface-mounted PM configuration and is much easier to make and cool since the PMs are physically separately from the armature windings but remain stationary.

This paper is organized as follows. The operation principle of the proposed PS-FRPM machine will be introduced in section II. In section III, the PS-FRPM machines are globally optimized and the influence of stator and rotor pole number combination as well as the other leading design parameters on the torque density is highlighted. In section IV, PS-FRPM machines are quantitatively compared with the conventional FRPM machine in terms of torque characteristics when both types of machines are globally optimized. The experimental validation based on two prototype machines is presented in section V followed by the conclusions.

II. Operation Principle

The proposed 12/10-stator/rotor-pole PS-FRPM machine is illustrated in Fig. 1(b). The 3-phase non-overlapping concentrated armature windings are wound on the outer stator and the PMs are surface-mounted in the inner stator. Hence, PMs and armature windings are physically separated. The inner stator with surface-mounted PMs is similar to the rotor of a conventional surface-mounted PM machine [1]. Therefore, it is easy to mount the PMs in PS-FRPM machine. Furthermore, the number of magnets in PS-FRPM machine is half of the magnet number in conventional FRPM machines, since the adjacent two PMs having the same polarity become one single piece. This further eases the manufacturing. Between the outer stator and the inner stator, the rotor iron pieces are sandwiched.

This article has been accepted for publication in a future issue of this journal, but has not been fully edited. Content may change prior to final publication. Citation information: DOI 10.1109/TMAG.2014.2358199, IEEE Transactions on Magnetics

Despite various differences between the PS-FRPM and conventional FRPM machines, they still share the same operation principle. In PS-FRPM machine, the rotor position θ_e in electric degrees can be given by (1), where N_r is rotor pole number and θ_m is rotor position in mechanical degrees.

$$\theta_e = N_r \theta_m \quad (1)$$

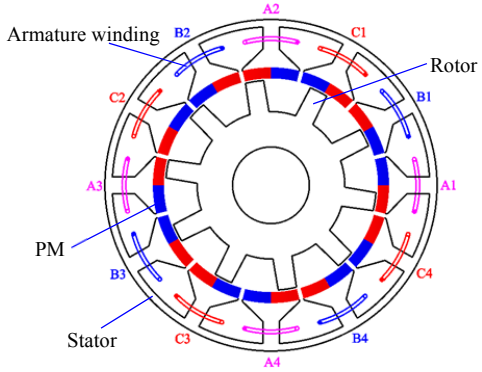

(a) Conventional FRPM machine

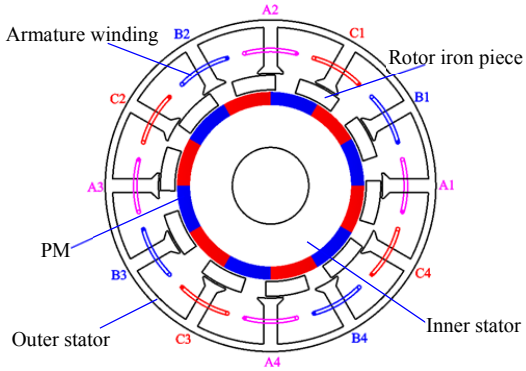

(b) Proposed PS-FRPM machine

Fig. 1 Cross-section of 12/10-pole conventional FRPM and proposed PS-FRPM machines.

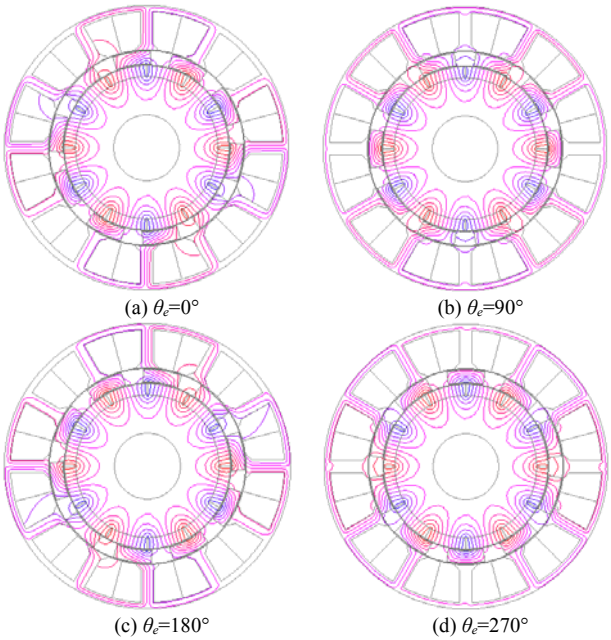

(a) θ_e=0° (b) θ_e=90° (c) θ_e=180° (d) θ_e=270°

Fig. 2 Open-circuit flux distributions of 12/10 stator/rotor-pole PS-FRPM machine at four typical rotor positions.

For a 12/10 stator/rotor pole PS-FRPM machine, as shown in Fig. 2(a), when θ_e=0, the phase A flux-linkage of Φ_A reaches positive maximum. After the rotor rotates to 90° electric degrees, Fig. 2(b), the PM flux is short-circuited and Φ_A=0. When θ_e=180°, Fig. 2(c), Φ_A becomes negative maximum. Φ_A is 0 again when θ_e=270°, Fig. 2(d). Therefore, a bipolar phase flux-linkage can be obtained in a PS-FRPM machine.

The flux-linkage waveforms and spectra of coils A1, A2 and their sum (half of phase A) of the 12/10-pole PS-FRPM machine are shown in Fig. 3. N_c is the number of turns in each armature coil. Although there are even flux-linkage harmonics in coils A1 and A2, they will be cancelled when A1 and A2 are connected in series.

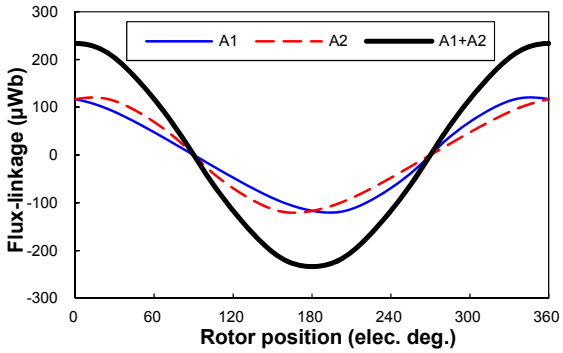

(a) Waveforms

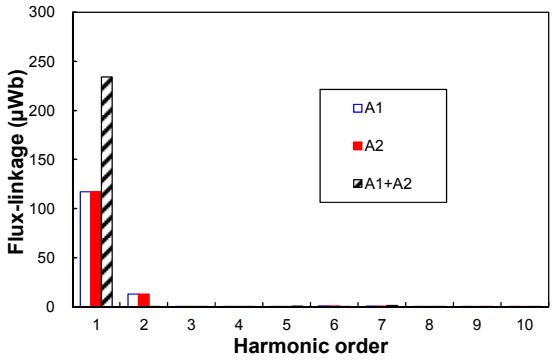

(b) Spectra

Fig. 3 Flux-linkages of coils A1, A2 and their sum (half of phase A) in 12/10-pole PS-FRPM machine, N_c=1.

III. Optimal Designs and Influence of Leading Design Parameters

The influence of stator and rotor pole number combinations on electromagnetic performance is investigated based on 12-stator-pole PS-FRPM machines. Theoretically, for a 3-phase machine, there are a lot of feasible combinations of stator and rotor pole numbers in PS-FRPM machines. For N_s/N_r-stator/rotor-pole PS-FRPM machine, the pitch factor of each coil can be given by (2), in which the fundamental pitch factor k_{pv} increases when the stator and rotor pole numbers differ less. Therefore, to obtain a larger fundamental pitch factor, 12-stator-pole PS-FRPM machines having 10-, 11-, 13- and 14-rotor-pole are selected for analysis in this section.

$$k_{pv} = \cos[v\pi(\frac{N_r}{N_s} - 1)] \quad (2)$$

where v is the harmonic order. N_s is the stator pole number.

In order to connect the armature coils belong to the same

This article has been accepted for publication in a future issue of this journal, but has not been fully edited. Content may change prior to final publication. Citation information: DOI 10.1109/TMAG.2014.2358199, IEEE Transactions on Magnetics

phase appropriately, coil back-EMF vectors of these four PS-FRPM machines are obtained and shown in Fig. 4. The open-circuit flux distributions of these optimal designs are given in Fig. 5.

All these four 12-stator-pole PS-FRPM machines are globally optimized for the maximum torque when having 45mm outer radius, 10.4mm inner radius, 25mm effective axial length, 20W rated copper loss. It should be noted that for a fair comparison, the PM volume of PS-SPM machines are set to be the same with the conventional 12/10-pole FRPM machine. The parameters of the conventional 12/10-pole FRPM machine will be given later.

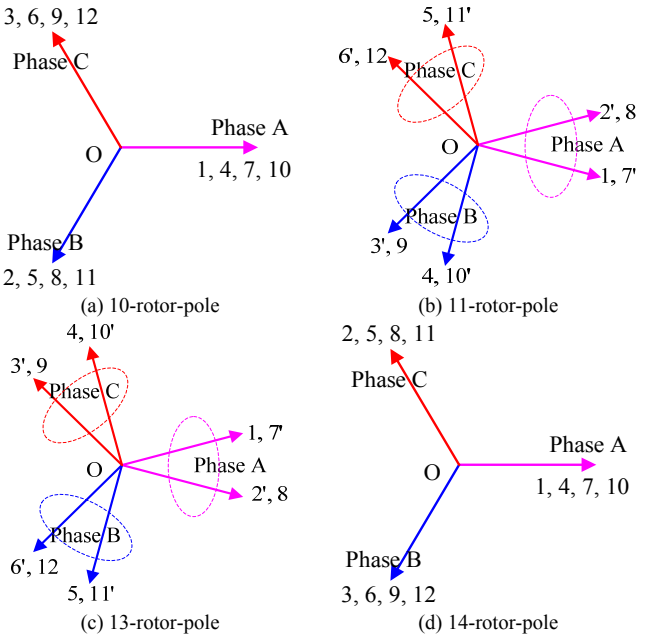

Fig. 4. Coil back-EMF vectors for 12-stator-pole PS-FRPM machines with different rotor pole numbers.

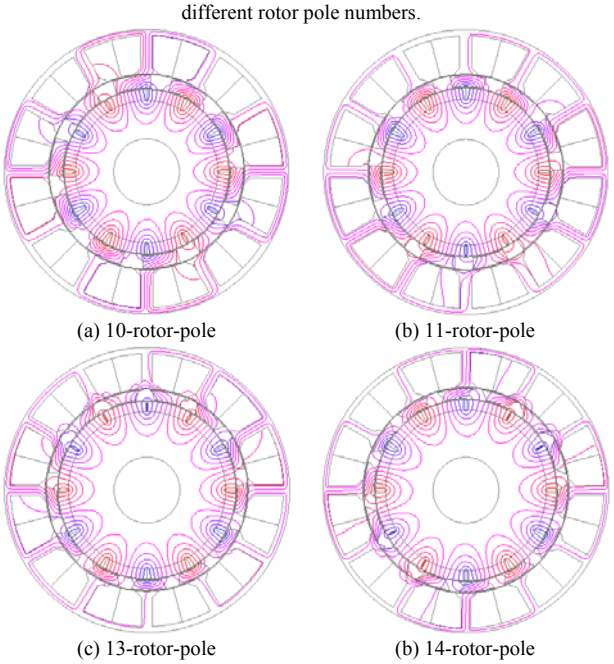

Fig. 5. Open-circuit flux distributions of 12-stator-pole PS-FRPM machines with different rotor pole numbers (θ_e=0°).

The design parameters of the PS-FRPM machines are illustrated in Fig. 6 while their optimal values are listed in TABLE I. In TABLE I, the parameters from L_{ef} to l_{otb} are fixed, as well as θ_{PM}=30°, whilst those from R_{osy} to θ_{ri} are globally optimized parameters. The influence of leading design parameters, such as air-gap radius, rotor pole radial thickness and pole arcs, on the electromagnetic torques in 12-stator-pole PS-FRPM machines with 10-, 11-, 13- and 14-rotor-poles are illustrated and analyzed as follows.

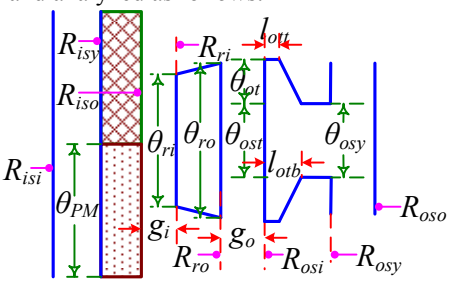

Fig. 6 Illustration of design parameters in PS-FRPM machine.

TABLE I

DESIGN PARAMETERS OF 12-STATOR-POLE PS-FRPM MACHINES

Parameters	Unit	Value			
Rotor pole number, N_r	-	10	11	13	14
Effective axial length, L_{ef}	mm	25			
Outer stator outer radius, R_{oso}	mm	45			
Inner stator inner radius, R_{isi}	mm	10.4			
Outer air-gap width, g_o	mm	0.5			
Inner air-gap width, g_i	mm	0.5			
Outer stator tip top length, l_{ott}	mm	0.5			
Outer stator tip bottom length, l_{otb}	mm	2			
PM arc, θ_{PM}	°	30			
Outer stator yoke radius, R_{osy}	mm	43	43	43	43.5
Outer stator inner radius, R_{osi}	mm	31	31	32	32.5
Rotor inner edge radius, R_{ri}	mm	26.5	27	28.5	29
Outer stator tooth arc, θ_{ost}	°	7	7	6	5
Outer stator tip arc, θ_{ot}	°	3	3	3	3
Rotor piece outer edge arc, θ_{ro}	°	23	22	20	20
Rotor piece inner edge arc, θ_{ri}	°	24	21	16	13

The influence of split ratio, which is defined in (3), on the torque of PS-FRPM machines is shown in Fig. 7.

$$\gamma = \frac{R_{go}}{R_{oso}} \tag{3}$$

where R_{go} is the radius of outer air-gap.

A larger split ratio will reduce the armature slot area and hence the electrical load but increase the air-gap diameter and PM flux. Hence, for all the combinations, the torque increases first and then decreases with the split ratio, as shown in Fig. 7. The optimal split ratio increases slightly with the rotor pole number. However, for all the four machines, the optimal split ratios are close to 0.7.

This article has been accepted for publication in a future issue of this journal, but has not been fully edited. Content may change prior to final publication. Citation information: DOI 10.1109/TMAG.2014.2358199, IEEE Transactions on Magnetics

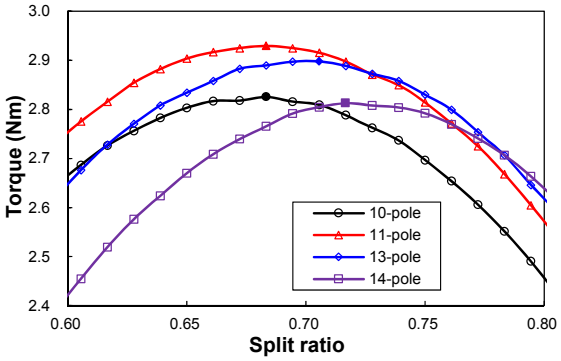

Fig. 7 Average electromagnetic torque variation with split ratio.

Fig. 8 shows the relationship between the average electromagnetic torque and the rotor radial thickness in PS-FRPM machines. It can be observed that the optimal rotor radial thickness is smaller when the rotor pole number is higher. The optimal rotor radial thickness is 4 mm for the 10-pole machine, 3.5 mm for the 11-pole machine, and 3 mm for the 13- and 14-pole machines.

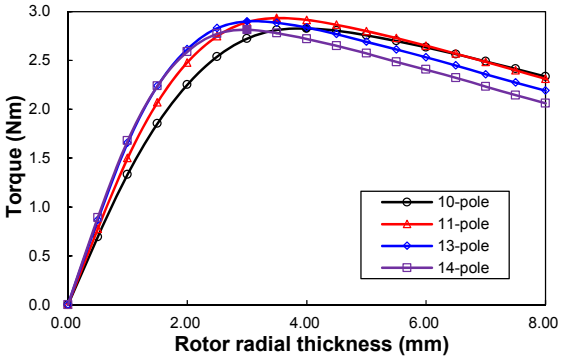

Fig. 8 Average electromagnetic torque variation and rotor radial thickness.

In PS-FRPM machines, the flux leakage between outer stator teeth is higher if the slot opening is smaller. However, the flux focusing effect will be less if the slot opening is bigger. As shown in Fig. 9, for 12-stator-pole with 10-, 11-, 13- and 14-rotor-pole PS-FRPM machines, the optimal outer stator slot opening ratio, which is defined as the the ratio of the slot opening to the stator pitch of the outer stator, is ~0.6. This optimal slot opening in PS-FRPM machines are significantly larger than the optimal slot opening in the conventional 12/10-pole FRPM machine shown in Fig. 1(a) since the PM width in conventional FRPM machine is linked to the slot opening whilst it is independent in PS-FRPM machine.

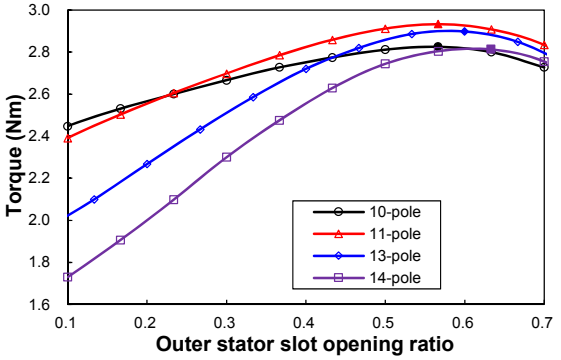

Fig. 9 Average electromagnetic torque against slot opening in outer stator.

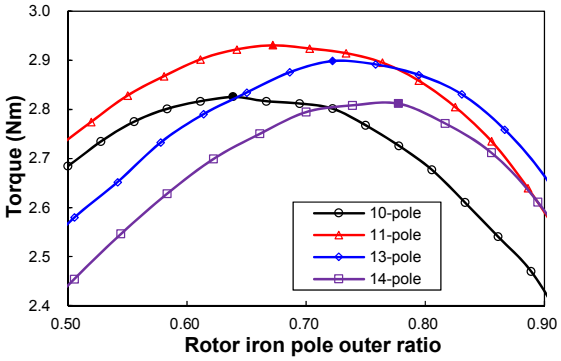

Fig. 10 Average electromagnetic torque variation with rotor outer iron pole arc ratio.

Figs. 10 and 11 show the relationships between the electromagnetic torque and the rotor outer and inner iron pole arc ratios which are defined as the ratio of rotor pole arc to the rotor pitch, respectively. Obviously, flux focusing effect will be less with smaller iron pole arc ratios, whilst larger iron pole arc ratios will result in more flux leakage between rotor iron pieces. As shown in Fig. 10, the optimal rotor outer iron pole arc ratio increases with the rotor pole number, *viz*. 0.64, 0.67, 0.72, and 0.78 for 10-, 11-, 13- and 14-rotor pole machines, respectively. For the rotor inner iron pole arc ratios, they are 0.67, 0.67, 0.57 and 0.51, respectively.

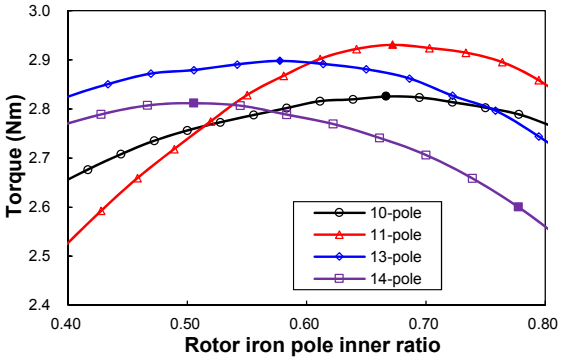

Fig. 11 Average electromagnetic torque variation with rotor inner iron pole arc ratio.

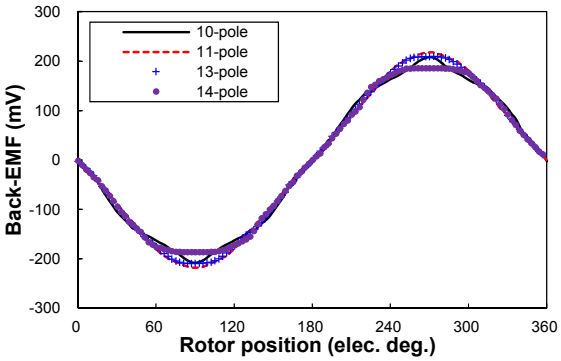

(a) Waveform

This article has been accepted for publication in a future issue of this journal, but has not been fully edited. Content may change prior to final publication. Citation information: DOI 10.1109/TMAG.2014.2358199, IEEE Transactions on Magnetics

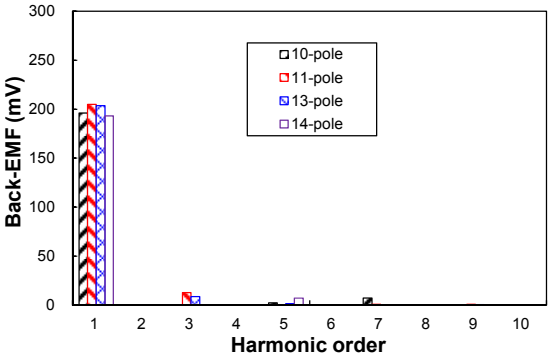

(b) Spectra

Fig. 12 Phase back-EMF of PS-FRPM machines, N_c=1 @400rpm.

With all the PS-FRPM machines globally optimized, Figs. 12 and 13 show the phase back-EMF and cogging torque of the optimal designs. As shown in Fig. 12(b), the 12/11-pole and 12/13-pole PS-FRPM machines exhibit larger fundamental back EMF, which implies that the 12/11- and 12/13-pole machines will potentially generate larger torque since as in the conventional FRPM machines the reluctance torque is negligible in PS-FRPM machines. Although 12/11- and 12/13-pole PS-FRPM machines have a 3rd harmonic, it will be eliminated in the line back-EMFs when Y-type winding connection is employed. For the 12/10- and 12/14-pole PS-FRPM machines, they have larger 5th and 7th harmonics, which implies larger torque ripples, than 11- and 13-pole machines. The PMs in PS-FRPM machines result in cogging torque which will cause torque ripple, acoustic noise and vibration. As shown in Fig. 13, the cogging torques in 10- and 14-pole machines are larger than those of 11- and 13-rotor-pole PS-FRPM machines. The reason is the larger 'goodness' factor, which is defined as the greatest common divisor of the stator slot number N_s and the rotor pole number N_r [13], in 10- and 14-pole machines.

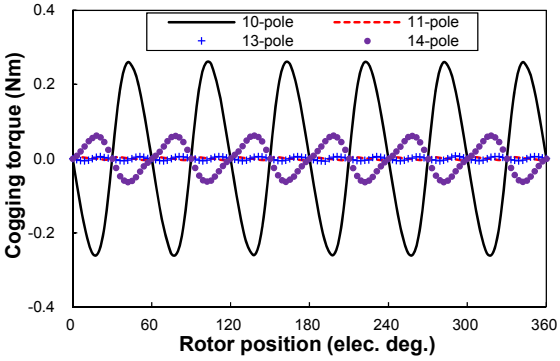

(a) Waveform

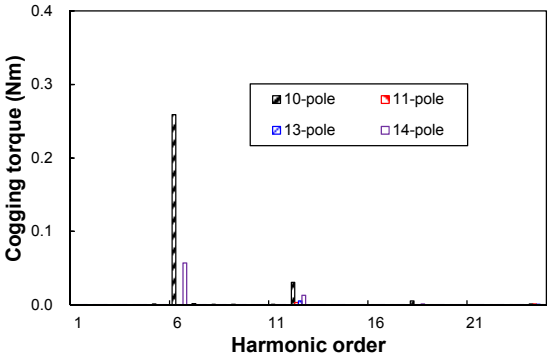

(b) Spectra

Fig. 13 Cogging torque of PS-FRPM machines.

IV. Comparison of Torque Characteristics between Proposed PS-FRPM and Conventional FRPM Machines

In this section, the torque characteristics of the proposed 12-stator-pole PS-FRPM machines and the conventional 12/10-pole FRPM machine with single stator will be comprehensively compared. The 12/10-pole FRPM machine is also globally optimized for the largest average torque with the same outer radius 45mm, inner radius 10.4mm, effective axial length 25mm and rated copper loss 20W as PS-FRPM machines. It should be noted that for the 12/10-pole conventional FRPM machine, the optimal PM thickness should be 1.5mm and the average torque is 1.89Nm if the design parameters are globally optimized, which will be shown later. However, the 1.5mm thick PMs will be irreversibly demagnetized and also are mechanically too fragile. In order to avoid these, the PM thickness is chosen to be 3mm (13414.6 mm^3 PM volume) to avoid these problems while other parameters are globally optimized. The globally optimised parameters based on 3mm PM thickness are stator yoke radius R_{sy}=43mm, stator inner radius R_{si}=32mm, stator tooth arc θ_{st}=8°, stator tip arc θ_{stip}=10°, and rotor pole arc θ_{rp}=10°.

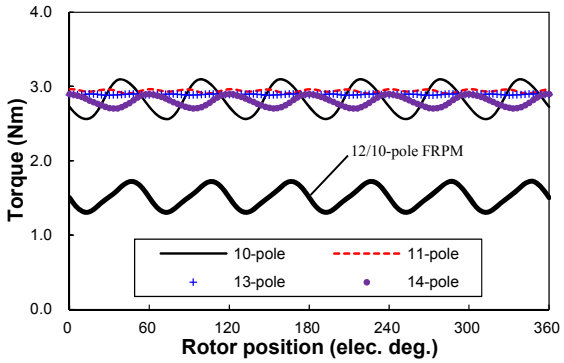

Fig. 14 Rated electromagnetic torque waveforms.

This article has been accepted for publication in a future issue of this journal, but has not been fully edited. Content may change prior to final publication. Citation information: DOI 10.1109/TMAG.2014.2358199, IEEE Transactions on Magnetics

TABLE II

TORQUE CHARACTERISTICS OF 12-STATOR-POLE PS-FRPM AND 12/10-POLE FRPM MACHINES

Item	12-stator-pole PS-FRPM				FRPM
N_r	10	11	13	14	10
T_{max} (Nm)	3.10	2.96	2.90	2.90	1.72
T_{min} (Nm)	2.56	2.91	2.88	2.71	1.31
T_{avg} (Nm)	2.83	2.94	2.89	2.81	1.51
T_r (%)	18.95	1.87	0.62	6.96	27.65

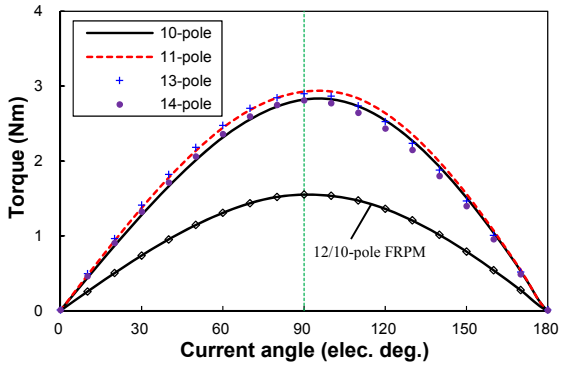

Fig. 15 Variation of average electromagnetic torque against current angle in 12-stator-pole PS-FRPM machines with different rotor pole numbers and 12/10-pole FRPM machine.

In order to compare the torque ripple of the four analyzed PS-FRPM machines and the conventional FRPM machine, the torque ripple coefficient is given by,

$$T_r = \frac{T_{max} - T_{min}}{T_{avg}} \times 100\% \qquad (4)$$

where T_{max}, T_{min} and T_{avg} are maximum, minimum and average electromagnetic torques, respectively.

In Fig. 14 and TABLE II, 11- and 13-rotor-pole PS-FRPM machines exhibit larger torque density, due to the larger fundamental back-EMF values as aforementioned in Fig. 12(a). The 10- and 14-pole PS-FRPM machines have larger torque ripple than 11- and 13-pole PS-FRPM machines since the 10- and 14-pole machines have larger 5th and 7th back-EMF harmonics, Fig. 12(b), as well as higher cogging torque, Fig. 13(a). As shown in Fig. 15, all PS-FRPM and FRPM machines in this paper reach the maximum torque when the current angle is approximately 90 degrees, *i.e.* zero *d*-axis current due to negligible reluctance torque. Hence, all the machines are optimized at i_d=0. The variation of average electromagnetic torque with the copper loss is shown in Fig. 16. Over the whole investigated copper loss range, the 11- and 13-rotor pole PS-FRPM machines always exhibit larger electromagnetic torque than the 10- and 14-rotor pole PS-FRPM machines. More importantly, all the PS-FRPM machines exhibit much larger torque density than the conventional 12/10-pole FRPM machine having single stator and the same PM volume.

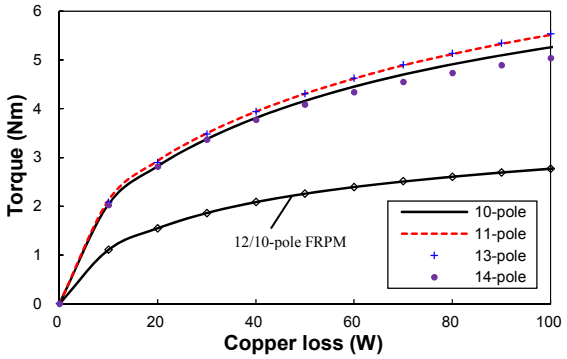

Fig. 16 Variation of electromagnetic torque against copper loss in 12-stator-pole PS-FRPM machines with different rotor pole numbers and 12/10-pole FRPM machine.

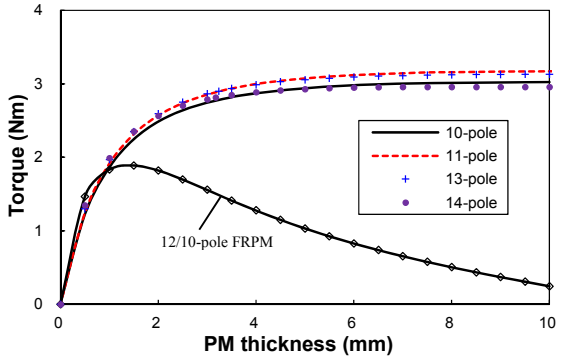

Fig. 17 Electromagnetic torque against PM thickness in 12-stator-pole PS-FRPM machines with different rotor pole numbers and 12/10-pole FRPM machine.

As aforementioned, in the conventional 12/10-pole FRPM machine, the PM thickness is not the optimal value in terms of the torque density. In this part, the influence of PM thickness on the torque density is also investigated in both the PS-FRPM and conventional FRPM machines when all the other parameters remain the same as the optimal values listed in TABLE I. The variation of the average torque with the PM thickness is shown in Fig. 17. It shows that the average electromagnetic torque in PS-FRPM machines increases and then saturates with the PM thickness. However, for the conventional FRPM machine, the torque first increases and then decreases when the PM thickness is higher since the PMs will directly affect the stator slot area and the rotor outer diameter, however these have been overcome in the proposed PS-FRPM machines due to partitioned stator and physical separation of armature windings and PMs. In order to further numerically explain these phenomena, the flux density variation on the outer stator tooth surface of the 12/10-pole conventional FRPM and PS-FRPM machines are obtained and analyzed when the rotor is at the position for the maximum A-phase flux linkage. As shown in Fig. 18, in order to illustrate the variation more clearly, the two tooth edges are designated as -1 and 1, respectively. For the conventional FRPM machine, both positive and negative parts of the radial flux density increase with the PM thickness. However, the negative part rises more quickly than positive part when the PM thickness is larger than 1mm. Therefore, the phase flux-linkage and hence the back-EMF fundamental magnitude will exhibit a maximum when the PM thickness varies. As shown in Fig. 17,

This article has been accepted for publication in a future issue of this journal, but has not been fully edited. Content may change prior to final publication. Citation information: DOI 10.1109/TMAG.2014.2358199, IEEE Transactions on Magnetics

when the PM thickness is 1.5mm, the conventional 12/10-pole FRPM machine exhibits the largest torque. However, taking mechanical strength and irreversible demagnetization into consideration, the PM thickness is designed to be 3mm as aforementioned. Different from the conventional FRPM machine with opposite polarity PMs mounted on teeth surface, the PMs in PS-FRPM machines are moved onto the inner stator. The radial flux density of the teeth surface and hence the torque always increase with PM thickness, as shown in Figs. 18 and 20.

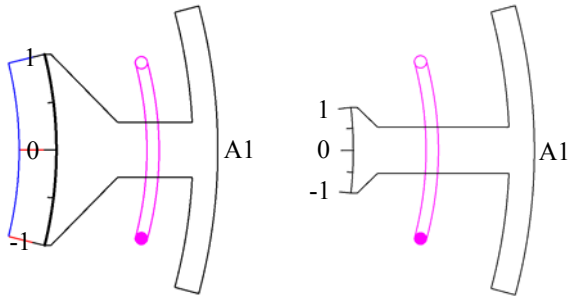

(a) FRPM (b) PS-FRPM

Fig. 18 Illustration of the radial flux density paths in 12/10-pole FRPM and PS-FRPM machines.

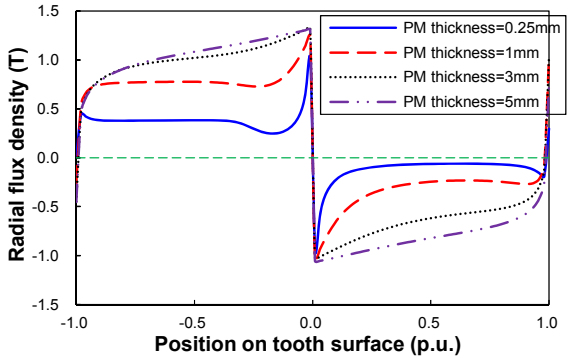

Fig. 19 Radial flux density waveforms on the surface of tooth corresponding to coil A1 in 12/10-pole FRPM machine (θ_e=0°).

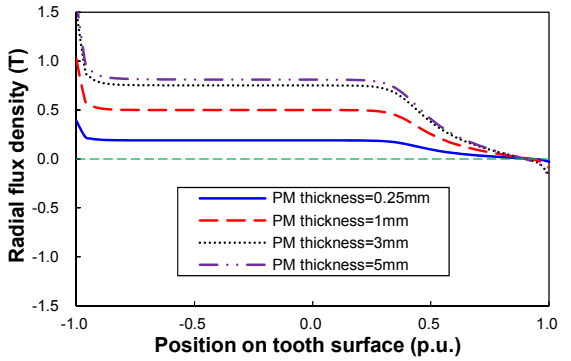

Fig. 20 Radial flux density waveforms on the surface of tooth corresponding of coil A1 in 12/10-pole PS-FRPM machine (θ_e=0°).

Since PMs in PS-FRPM machines have smaller radius than the one of the FRPM machine, PM thickness in PS-FRPM machines is larger than 3mm as shown in TABLE I when the PM volume is the same. As given in Fig. 17, the conventional 12/10-pole FRPM machine having 3mm thick PMs produces 1.55Nm torque. However, the proposed PS-FRPM machines having the same PM volume can produce more than 2.81Nm torque, which is ~181% of that in the conventional 12/10-pole FRPM machine. Without considering the mechanical stress and demagnetization, as shown in Fig. 17, the conventional 12/10-pole FRPM machine has the largest torque 1.89Nm when the PM thickness is 1.5mm. However, the proposed 12/10-pole PS-FRPM machines can produce more than 2.95Nm as shown in Fig. 17. Therefore, it can also be concluded the torque density of PS-FRPM machine can be 56% higher than that of the conventional FRPM machine.

V. Experimental Validation

Two PS-FRPM prototype machines are manufactured to verify the above analyses and shown in Fig. 21. Both prototype machines share the same partitioned stators, *i.e.* outer and inner stators. The dimensions of the prototype machines are listed in TABLE III. In order to ease the prototyping, additional lamination bridges between rotor poles are employed adjacent to the inner surface. T_{bri} in TABLE III is the thickness of the lamination bridges between rotor iron pieces. Thus, all the rotor poles are mechanically connected to obtain enough mechanical strength and relieve the tolerance requirement. The PM thickness is also rounded to 4mm. Electromagnetic performance of the prototype machines are predicted by 2D FE analysis and compared with the measures results including the back-EMFs and the static torques.

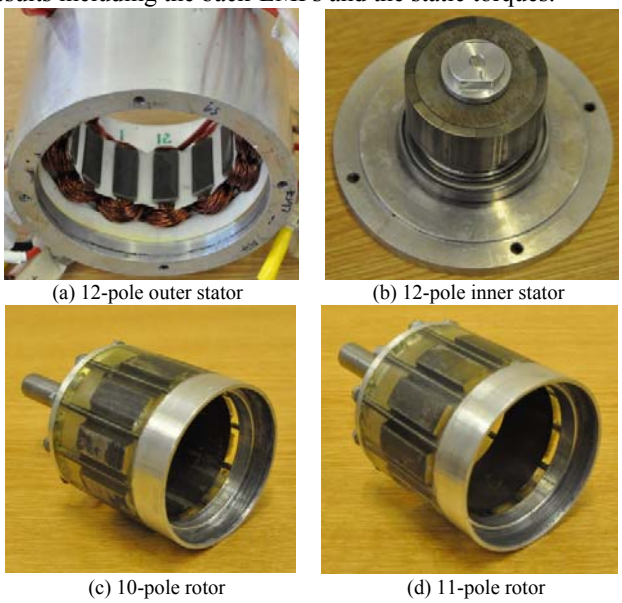

(a) 12-pole outer stator (b) 12-pole inner stator

(c) 10-pole rotor (d) 11-pole rotor

Fig. 21 12/10-pole and 12/11-pole prototype PS-FRPM machines.

As shown in Fig. 22, although the phase back-EMFs calculated by 2D FE are slightly higher than those of measurements due to the end effect, good agreements are achieved. The variation of static torque with the rotor position for PS-FRPM prototype machines is shown in Fig. 23. In 12/10-pole PS-FRPM prototype machine, good agreements between the 2D FE predicted and measured static torques under I_a=5A can be achieved. The difference slight increases when I_a=10A and I_a=15A due to stronger end effects. For the 12/11-pole PS-FRPM prototype machine, there is a 3rd torque harmonic in measured static torque, which is caused by the imperfect manufacturing. Fig. 24 shows the variation of 2D FE predicted and measured peak torques with the armature

This article has been accepted for publication in a future issue of this journal, but has not been fully edited. Content may change prior to final publication. Citation information: DOI 10.1109/TMAG.2014.2358199, IEEE Transactions on Magnetics

current. Again, good agreements are obtained despite of slightly difference due to the end effect in the 12/10-pole PS-FRPM machine. For the 12/11-pole PS-FRPM machine, the measured and 2D FE predicted peak torques are nearly the same. Although the end effect may lead to a slightly smaller measured peak torque than the 2D FE predicted one. However, the measured 3rd torque harmonic which is caused by imperfect manufacturing of the 11-pole rotor causes a higher measured peak torque, as shown in Fig. 23. Consequently, the measured and 2D FE predicted peak torques are approximately same as in the 12/11-pole PS-FRPM machine. It should be noted that as shown in Fig. 24, 2D FE predicted peak torque in the 10-pole PS-FRPM prototype machine is higher than the 11-pole one. This is because the values of design parameters of the prototype machine are not the same as the globally optimized ones, for easing the prototyping.

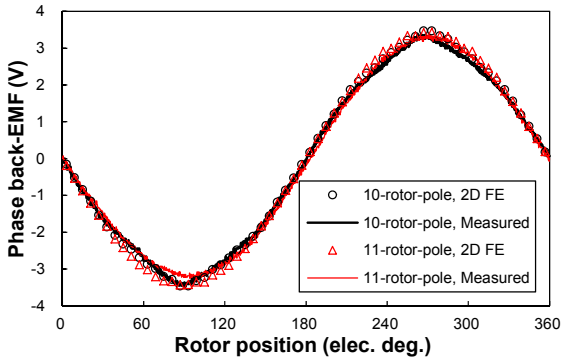

Fig. 22 Variation of 2D FE predicted and measured phase back-EMFs with rotor position in the prototype machines.

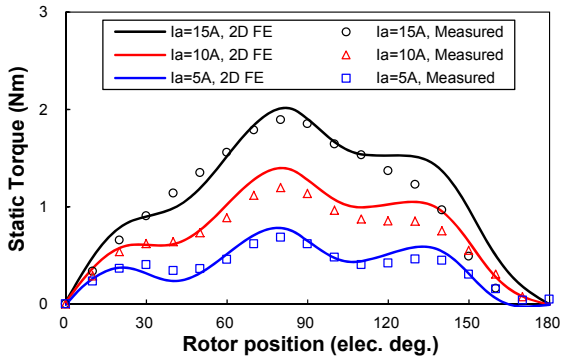

(a) 10-rotor-pole

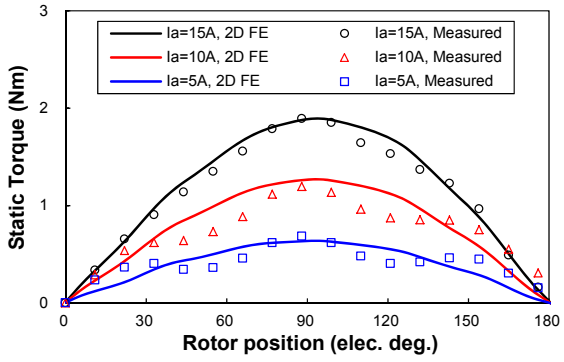

(b) 11-rotor-pole

Fig. 23 Variation of 2D FE predicted and measured static torque with rotor position (I_a=-2I_b=-2I_c).

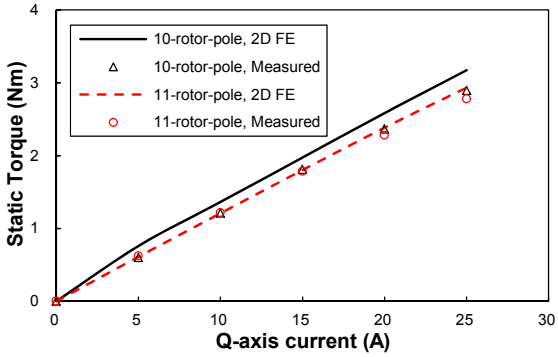

Fig. 24 Variation of 2D FE predicted and measured peak torque with armature current of the prototype machines.

TABLE III
DESIGN PARAMETERS OF 12-STATOR-POLE PS-FRPM PROTOTYPE MACHINES

Parameters	Prototype Machines		Parameters	Prototype Machines	
N_r	10	11	N_r	10	11
L_a (mm)	25		g_o (mm)	0.5	
R_{oso} (mm)	45		g_i (mm)	0.5	
R_{osy} (mm)	42		θ_{ost} (°)	8.12	
R_{osi} (mm)	31.75		θ_{osy} (°)	6.14	
R_{ro} (mm)	31.25		θ_{ot} (°)	4.94	
R_{ri} (mm)	26.15		l_{ott} (mm)	1	
R_{iso} (mm)	25.75		l_{otb} (mm)	3	
R_{isy} (mm)	21.75		θ_{ro} (°)	18	20
R_{isi} (mm)	10.4		θ_{ri} (°)	24	22.7
T_{PM} (mm)	4		θ_{PM} (°)	30	
T_{bri} (mm)	0.5				

VI. CONCLUSIONS

In this paper, a novel type of PS-FRPM machine with partitioned stator is proposed, in which PMs and armature windings are separately located in the inner and outer stators, respectively. Compared with the conventional FRPM machine having single stator, the proposed PS-FRPM machines can exhibit ~56% higher torque capability. The influence of rotor pole numbers in a 12-stator-pole PS-FRPM machine is investigated. It shows that amongst 12/10, 12/11, 12/13 and 12/14 stator/rotor-pole PS-FRPM machines, 11-pole and 13-pole machines exhibit larger back-EMF and hence electromagnetic torque as well as lower cogging torque and torque ripple, albeit with potentially higher unbalanced magnetic force due to odd rotor pole numbers. In addition, the influence of leading design parameters is also investigated. It shows that in PS-FRPM machines electromagnetic torque increases and saturates with the PM thickness, whilst for the conventional FRPM machines, there will be an optimal PM thickness for maximum torque.

Acknowledgement

The authors acknowledge the financial support received from the Royal Academy of Engineering and Siemens Wind Power.

VII. REFERENCES

[1] Z. Q. Zhu, and D. Howe, "Electrical machines and drives for electric, hybrid and fuel cell vehicles," *Proc. IEEE*, vol. 95, no. 4, pp. 746-765, Apr. 2007.

[2] Z.Q. Zhu, "Switched flux permanent magnet machines – innovation continues", *Keynote Speech, Proc. of Int. Conf. on Electrical Machines and Systems* (ICEMS2011), 2011, Beijing, paper Keynote Speech-06, pp.1-10.

[3] M. Cheng, W. Hua, J. Z. Zhang, and W. X. Zhao, "Overview of stator-permanent magnet brushless machines," *IEEE Trans. Indus. Electron.*, vol. 58, no. 11, pp. 5087-5101, Nov. 2011.

[4] Y. Liao, F. Liang, and T. A. Lipo, "A novel permanent-magnet motor with doubly-salient structure," *IEEE Trans. Ind. Appl.*, vol. 31, pp. 1069–1078, Sep./Oct. 1995.

[5] D. Wu, J. T. Shi, Z. Q. Zhu, and X. Liu, "Electromagnetic performance of novel synchronous machines with permanent magnets in stator yoke," *IEEE Trans. Magn.*, in press.

[6] Z. Q. Zhu, Y. Pang, D. Howe, S. Iwasaki, R. Deodhar, and A. Pride, "Analysis of electromagnetic performance of switched flux switching permanent magnet machines by non-linear adaptive lumped parameter magnetic circuit model," *IEEE Trans. Magn.*, vol. 41, no. 11, pp. 4277–4287, Nov. 2005.

[7] Z. Q. Zhu, A. S. Thomas, J. T. Chen, and G. W. Jewell, "Cogging torque in flux-switching permanent magnet machines," *IEEE Trans. Magn.*, vol. 45, no. 10, pp. 4708-4711, Oct. 2009.

[8] C. X. Wang, I. Boldea, and S. A. Nasar, "Characterization of three phase flux reversal machine as an automotive generator," *IEEE Trans. Energy Convers.*, vol. 16, no. 1, pp. 74-80, Mar. 2001.

[9] A. Toba, and T. A. Lipo, "Novel dual-excitation permanent magnet Vernier machine," in *Proc. IEEE IAS Annu. Conf.,* Phoenix, USA, 1999, vol. 4, pp. 2539-2544.

[10] M. Abbasian, M. Moallem, and B. Fahimi, "Double-stator switched reluctance machines (DSSRM): fundamentals and magnetic force analysis," *IEEE Trans. Energy Convers.*, vol. 25, no. 3, pp. 589-597, Sep. 2010.

[11] Y. B. Wang, M. Cheng, Y. Du, and K. T. Chau, "Design of high-torque-density double-stator permanent magnet brushless motors," *IET Electr. Power Appl.*, vol. 5, no. 3, pp. 317-323, Mar. 2011.

[12] Z. Y. Zong, L. Quan, Y. M. Ge, "A new double-stator flux-switching permanent magnet machine for electric vehicle application," in *Rec. of IEEE Inter. Magn. Conf.*, Dresden, Germany, 2014, pp. GP-5.

[13] Z.Q. Zhu, and D. Howe, "Influence of design parameters on cogging torque in permanent magnet machines," *IEEE Trans. Energy Convers.*, vol.15, no.4, pp.407-412, Dec. 2000.